PHYSICAL REVIEW D **80,** 054503 (2009)

Numerical evidence of chiral magnetic effect in lattice gauge theory

P. V. Buividovich,[1,2] M. N. Chernodub,[3,4,2] E. V. Luschevskaya,[2] and M. I. Polikarpov[2]

[1]*JIPNR "Sosny," National Academy of Science, Acad. Krasin str. 99, Minsk, 220109 Belarus*
[2]*ITEP, B. Cheremushkinskaya 25, Moscow, 117218 Russia*
[3]*LMPT, CNRS UMR 6083, Fédération Denis Poisson, Université de Tours, 37200 France*
[4]*DMPA, University of Gent, Krijgslaan 281, S9, B-9000 Gent, Belgium*

(Received 12 July 2009; revised manuscript received 13 August 2009; published 21 September 2009)

The chiral magnetic effect is the generation of electric current of quarks along an external magnetic field in the background of topologically nontrivial gluon fields. There is recent evidence that this effect is observed by the STAR Collaboration in heavy-ion collisions at the Relativistic Heavy Ion Collider. In our paper we study qualitative signatures of the chiral magnetic effect using quenched lattice simulations. We find indications that the electric current is indeed enhanced in the direction of the magnetic field both in equilibrium configurations of the quantum gluon fields and in a smooth gluon background with nonzero topological charge. In the confinement phase the magnetic field enhances the local fluctuations of both the electric charge and chiral charge densities. In the deconfinement phase the effects of the magnetic field become smaller, possibly due to thermal screening. Using a simple model of a fireball we obtain a good agreement between our data and experimental results of STAR Collaboration.

DOI: 10.1103/PhysRevD.80.054503 PACS numbers: 12.38.Gc, 11.30.Rd, 13.40.−f

I. INTRODUCTION

Properties of strongly interacting matter in hadron-scale magnetic fields have attracted a lot of attention recently. The interest is motivated by the feasibility of creating such strong fields in ongoing heavy-ion experiments at the Relativistic Heavy Ion Collider (RHIC), and at future experiments at the Facility for Antiproton and Ion Research at GSI, and the ALICE experiment at LHC. Noncentral heavy-ion collisions may create magnetic fields due to relative motion of electrically charged ions and the products of the collision. For typical RHIC parameters the strength of the magnetic field at the center of a Au-Au collision may be estimated to be of the order of $eB \sim (10\text{–}100\ \mathrm{MeV})^2$ [1] at the first moments ($\tau \sim 1\ \mathrm{fm/c}$) of the collision. The magnetic field created at RHIC is not only many orders of magnitude stronger than any other experiment may reach, it also leaves behind even magnetized neutron stars, magnetars, with their magnetic fields of the order of 10^{10} T (equivalent to $eB \approx 4\ \mathrm{MeV}^2$). A strong magnetic field can significantly modify the properties of nuclear matter affecting the spectrum of the hadronic states [2], shifting the position and changing the order of the phase transition from hadronic matter to quark-gluon plasma [3].

The magnetic fields lead to other unusual effects due to the nontrivial topological structure of QCD [1,4–6]. In this paper we concentrate on a particular realization of the chiral magnetic effect (CME), which generates a spatial separation of positive and negative *electric* charges along the direction of the *magnetic* field on nontrivial topological backgrounds of gluons [1,4]. In the noncentral collisions the magnetic field is perpendicular to the reaction plane, therefore a charge separation can be observed in heavy-ion collisions as a nonstatistical asymmetry in the number of positively and negatively charged particles emitted on different sides of the reaction plane [7,8]. This effect was called "event-by-event P and CP violation," because this asymmetry implies that the difference of the numbers of quarks of different chiralities was created in a particular event due to quantum fluctuations of the topological charge. However, since there is no CP violation in strong interactions in the usual sense, this effect vanishes after averaging over all events. The only way to observe it experimentally is by studying CP-even correlations of reaction products [7]. The magnetic field grows with the impact parameter of the collision, therefore this asymmetry should depend strongly on the centrality of the collision. There are preliminary indications that this effect has been indeed observed by the STAR Collaboration at RHIC [8,9]. It should be stressed that the observed effect is the indication that there are fluctuations of chirality in QCD vacuum. A similar well-known effect is the large mass of the η' meson [10,11]. However, the CME allows one to extract more information on the fluctuations of chirality and topological charge, since in this case there is an additional parameter—the strength of the magnetic field—which can be varied in experiments.

The physical mechanism behind the CME is as follows [1,4]. At the energy scales of the collisions, the light u and d quarks may be considered as approximately massless particles. The massless fermions are characterized by right- or left-handed helicity (i.e., positive or negative projection of fermion's spin on the momentum, respectively), so that the magnetic moment of the (anti)quark is always collinear to its momentum. The strong enough external magnetic field makes the magnetic moment to be parallel to the direction of the field so that the motion of the quarks is essentially collinear to the magnetic field.

 © 2009 The American Physical Society

The helicity is related to chirality: the quarks have the same helicity and chirality while for the antiquarks the helicity is opposite to chirality. In the equilibrium ensembles the total chirality is vanishing [12], so that the total electric current along the magnetic field is zero (the left-handed and right-handed quarks move in opposite directions and compensate each other). However, if there is a difference between the (anti)quarks with left- and right-handed chirality then the balance is broken and the total electric current along the magnetic field becomes nonzero [1,4–6,13,14].

Thus, the CME arises due to the fluctuations in the numbers of left- and right-handed quarks in a vacuum or in the thermal state of non-Abelian gauge theories. In QCD the fluctuations of the chirality number are provided by the topology-changing transitions between different vacua. Indeed, the gluon fields are characterized by the topological winding number [15,16]

$$Q = \frac{g^2}{16\pi^2}\int d^4x G_a^{\mu\nu}(x)\tilde{G}^a_{\mu\nu}(x), \qquad Q \in \mathbb{Z}, \tag{1}$$

where $G_a^{\mu\nu}$ is the gluon field strength tensor and the dual tensor is $\tilde{G}_a^{\mu\nu} = (1/2)\varepsilon^{\mu\nu\alpha\beta}G_{a,\alpha\beta}$. The configurations with $Q \neq 0$ change the chirality of the ensemble, i.e., the difference between the number of left-handed quarks (N_L) and right-handed quarks (N_R) by an integer

$$\Delta(N_L - N_R) = N_f Q, \tag{2}$$

where N_f is the number of flavors. Therefore the electric current along the strong enough magnetic field should be sensitive to the topological fluctuations of the gluon ensembles, providing us with possibility of studying in a direct way the topological structure of the QCD thermal states.

The CME is expected to work effectively in the chirally restored phase [1,4]: the chiral condensate, which breaks the chiral symmetry, provides a direct coupling between left-handed quarks to the right-handed ones thus leading to an efficient mechanism to suppress any asymmetry between them. The suppression happens because the system prefers to decrease total chirality as the states with nonzero chirality have higher energy due to the Fermi principle [12]. Therefore the CME should work effectively in the high temperature case, where the chiral condensate is suppressed and the chirality fluctuations are strong.

While there are many phenomenological estimates of the strength of the CME in QCD, a detailed analytical calculation is hardly possible due to strong nonperturbative effects. In this paper we report on our results of the numerical investigation of the CME in quenched $SU(2)$ lattice gauge theory both in high and low temperature phases of the theory (Sec. II). The chiral properties of the QCD, such as chiral condensate [17] and the chiral magnetization [18], in the external magnetic field can reasonably be described by the quenched lattice theory. Our study involves various approximations: we use quenched lattice gauge theory with two colors, the fermionic propagators are truncated, and the theory is studied in a finite volume. Thus our results should only serve as a qualitative indication of the existence of the CME, while the quantitative features may be accessible only in simulations with dynamical quarks. Using our numerical results we nevertheless make a prediction for the charge asymmetry and fit it to the experimental data in Sec. III. Our conclusions are summarized in the last section.

II. LATTICE SIMULATIONS

A. Numerical setup

We work in $SU(2)$ lattice gauge theory with tadpole-improved Wilson-Symanzik action (see, e.g., expression (1) in Ref. [19]). In our zero temperature simulations we have used 14^4 and 16^4 lattices at lattice spacing $a = 0.103$ fm and $a = 0.103$ fm, $a = 0.089$ fm, respectively. The latter lattices were used to control the effects of finite volume and finite lattice spacings, which turn out to be much less than the statistical errors. For simulations at finite temperature we have used $16^3 \times 6$ lattices with spacings $a = 0.128$ fm and $a = 0.095$ fm, which correspond to the temperatures $T = 256$ MeV $= 0.82T_c$ and $T = 350$ MeV $= 1.12T_c$, respectively. The critical temperature in $SU(2)$ gauge theory is $T_c = 313.(3)$ MeV [20]. As we explain below, the minimal nonzero value of the magnetic field is rather large in our simulations, $qB_{\min} \sim (350\ \text{MeV})^2$).

In all current lattice simulations with background magnetic field only valence quarks interact with the electromagnetic field [2,17,21,22], because the inclusion of dynamical sea quarks into simulations makes the problem significantly difficult. On the other hand the characteristic properties of the CME may be studied in the quenched approximation, in which the effects of the virtual quarks on the gluon fields are neglected.

The quenched world has the same qualitative features as the unquenched system: both approaches exhibit color confinement and chiral symmetry breaking. There is, however, an important difference: due to the Crewther theorem [23] fluctuations of the net topological charge in the theory with light virtual quarks should be drastically suppressed compared to the quenched vacuum. However, as we have checked numerically, at least in the quenched approximation the CME is mostly due to local fluctuations of the density of topological charge, rather than due to the global topological charge of gauge field configurations. The number of colors is also inessential for the existence of the CME. Thus we proceed with the quenched simulations of the $SU(2)$ gauge theory on the lattice.

For valence quarks we use Neuberger's overlap Dirac operator [24]. The expectation values of fermionic fields are first computed in terms of a massive Dirac propagator in a fixed configuration of gauge fields, according to the Wick theorem. For example, for the expectation value

involving four fermionic fields in the background of a fixed gauge field A, one has

$$\langle \psi^\dagger(x) O_1 \psi(x) \psi^\dagger(x) O_2 \psi(x)\rangle_A = \mathrm{Tr}\left(\frac{1}{\mathcal{D}+m} O_1\right) \mathrm{Tr}\left(\frac{1}{\mathcal{D}+m} O_2\right) - \mathrm{Tr}\left(\frac{1}{\mathcal{D}+m} O_1 \frac{1}{\mathcal{D}+m} O_2\right), \tag{3}$$

where $\mathcal{D}$ is the massless Dirac operator on the lattice,

$$\mathcal{D} = \gamma^\mu(\partial_\mu - iA_\mu), \tag{4}$$

and O_i, $i = 1, 2$ are some operators in spinor and color space. These operators are treated as matrices in spinor and color spaces. Consequently, the traces in Eq. (3) are taken over both spinor and color indices.

The overlap operator is a vital tool for investigation of the CME because this effect is realized for the chiral quarks, while the overlap operator is the lattice Dirac operator which enjoys the chiral symmetry by the construction. On the contrary, if the quarks are massive then the chiral magnetic effect is overshadowed by the flips of the quarks' spirality. Moreover, in the CME the near-zero Euclidean eigenmodes play an essential role. The overlap operator gently treats low-lying eigenmodes making our results more reliable. On the other hand, this operator is more complicated compared to other versions of the lattice Dirac operators. As a result, the simulations are more power-consuming and our data have larger error bars.

The Dirac propagator $1/(\mathcal{D} + m)$ can be represented in terms of the eigenvalues λ_k and the eigenmodes ψ_k of the Dirac operator,

$$\mathcal{D}\,\psi_k = i\lambda_k \psi_k, \tag{5}$$

as follows:

$$\frac{1}{\mathcal{D}+m}(x, y) = \sum_k \frac{\psi_k(x)\psi_k^\dagger(y)}{i\lambda_k + m}. \tag{6}$$

Then Eq. (3) can be reformulated as follows:

$$\langle \bar\psi O_1 \psi \bar\psi O_2 \psi\rangle_A = \sum_{k,p} \frac{\langle k|O_1|k\rangle\langle p|O_2|p\rangle - \langle p|O_1|k\rangle\langle k|O_2|p\rangle}{(i\lambda_k + m)(i\lambda_p + m)}. \tag{7}$$

The result is then averaged over all configurations of the gauge fields. This procedure is repeated for several values of the mass m (we have used $m = 25$ MeV, $m = 50$ MeV, $m = 75$ MeV), and the obtained dependence on m is linearly extrapolated to zero to yield the expectation values in the chiral limit. In order to have a well-defined limit $m \to 0$, exact zero modes of the Dirac operator were not included in the Dirac propagator. The removal of zero modes is legal, since their contribution becomes insignificant in the limit $V \to \infty$, $m \to 0$ if one first tends the volume to infinity and then sets the mass to zero. The Dirac propagator is evaluated by inverting the massive Dirac operator in the subspace spanned by M Dirac eigenvectors which correspond to M nonzero Dirac eigenvalues with smallest absolute values. The truncated operator (6) reads as follows:

$$\frac{1}{\mathcal{D}+m}(x, y) = \sum_{|k|<M} \frac{\psi_k(x)\psi_k^\dagger(y)}{i\lambda_k + m}. \tag{8}$$

The value of M is limited by the numerical procedure (ARPACK in our case) used to find the eigensystem of the Dirac operator. We have found that the UV-finite quantities depend only weakly on M.

Uniform magnetic field with field strength $F_{12} = B$ is introduced into the Dirac operator by substituting the $su(2)$-valued vector potential A_μ with the $u(2)$-valued one,

$$A_{\mu ij} \to A_{\mu ij} + A_\mu^{(B)}\delta_{ij}, \qquad A_\mu^{(B)}(x) = \frac{B}{2}(x_1\delta_{\mu,2} - x_2\delta_{\mu,1}). \tag{9}$$

The expression (9) is valid in infinite space. In order to combine it with periodic boundary conditions on the lattice we have introduced an additional x-dependent boundary twist for fermions, as explained in [25]. Since the total magnetic flux is quantized, on finite periodic space with the period L the uniform magnetic field can take only discrete values

$$qB = \frac{2\pi k}{L^2}, \qquad k \in \mathbb{Z}, \tag{10}$$

where q is the quark charge. In our calculations we take $q = -e/3$, corresponding to the d quark. Because of the quantization condition (10) there is a minimal nonzero value of the magnetic field, which is equal to $\sqrt{qB} = 348$ MeV in most of our simulations (for 14^4 lattice with lattice spacing $a = 0.103$ fm one has $L = 14 \cdot a = 1.44$ fm).

In our work the spatial tensor indices are $i, j = 1, 2, 3$ and the Euclidean time is labeled by the index 4. The magnetic field $F_{12} = B_3 = B$ is uniform in our simulations; see Eq. (9).

B. Observables and topology

In order to characterize the CME quantitatively, we studied two basic quantities. The first quantity is the local chirality

$$\rho_5(x) = \bar\psi(x)\gamma_5\psi(x), \tag{11}$$

which is the operator of the difference of the local densities of left- and right-handed quarks.

The second quantity is the electromagnetic current

$$j_\mu(x) = \bar\psi(x)\gamma_\mu\psi(x). \tag{12}$$

All other studied quantities are the powers and the products

of (11) and (12). Note that in Euclidean space the spinor conjugation is just the complex conjugation $\bar{\psi}_{\rm Eucl} = \psi^\dagger$ [16].

According to the original idea of Refs. [1,4] the CME appears in the presence of the topologically nontrivial configurations. The nonzero topological charge is needed to destroy a balance between the left- and right-quark zero modes. In general, configurations of gauge fields may have different values of the global topological charge. According to the Atyah-Singer theorem, the topological charge of a gauge field configuration is given by a difference of the right and left zero modes of the Dirac operator,

$$N_L - N_R = Q \tag{13}$$

[this is essentially a Euclidean version of Eq. (2) written for one species of fermions, $N_f = 1$]. The crucial advantage of our numerical procedure is that we are using the chirally symmetric Dirac operator which possesses exact zero modes. The knowledge of the zero modes for a given gluon field allows us to calculate the integer-valued topological charge of this configuration using Eq. (13).

Surprisingly, we have observed that all studied CME-related observables are independent of the global charge of the gluon fields. More precisely, in the external magnetic field the effect of the nontrivial topology is smaller then the statistical error for any studied quantity like (11) and (12), their powers, and correlations. One could incorrectly conclude that the electromagnetic properties of the QCD vacuum in the external magnetic field have nothing to do with the topology of the gluon fields and, consequently, the CME is not realized in the (thermal) equilibrium (we remind the reader that the CME is an interplay between the electromagnetism and the gluon topology).

Coming a bit in advance, we state that the real situation turns out to be more complicated. In fact, each gauge field configuration contains quite strong *local* fluctuations of the topological charge. In the real equilibrium configurations of the gauge fields, the density of the topological charge is localized on low-dimensional objects [26] which do not resemble smooth structures like, for example, classical instantons. And, consequently, the effect of the global topology is completely overshadowed by strong local fluctuations of the topological charge. Thus, below we do not classify the gauge field configurations by the topological charge, treating all configurations on equal footing. On the contrary, our studies, reported in this paper, show that the CME does exist in equilibrium and that the magnetic fields do affect the electromagnetic properties of vacuum at *local* concentrations of the topological charge.

We prefer to study correlation of the electromagnetic current (12) with the chiral density (11). The chiral density is calculated with the help of the low eigenmodes of the Dirac operator in the background of the gauge field configuration, as described in the previous subsection. In fact, the CME predicts the correlation of the electromagnetic currents with the imbalanced density of the left- and right-quark zero modes. The exact zero modes of separate topological lumps in a configuration of the gluon fields (one can think, for example, of separate instantons and anti-instantons) become near-zero modes because of the interactions between the modes. This interaction breaks the zero-mode degeneracy and the former zero modes acquire tiny corrections. Such near-zero modes carry information about unperturbed zero modes including the distribution of chirality and, eventually, about the chiral magnetic effect.

In order to illustrate the insignificance of the exact Euclidean [27] zero modes let us consider a configuration consisting of an instanton–anti-instanton pair. Assume that these objects are separated by a distance which is much larger compared to their sizes, and this configuration has no zero fermion modes since the total topological charge is zero. If one applies an external magnetic field to this configuration, the lumps of the topological charge will be the sources of the generation of the electric current. At the instanton the electric current will be generated in one direction, while at the anti-instanton the current will start flowing in the opposite direction. The CME mechanism leads to the current generation because each of the (anti) instantons changes the chirality of quarks in the positive or negative direction, and the local imbalance of the chirality leads to a generation of the positive or negative current, respectively.

At the instanton–anti-instanton configuration the global electric current is zero, while locally each topological lump induces the electric currents exhibiting the CME. Therefore, we concentrate our attention on local correlators ignoring the global signatures of the CME like global currents and/or the Euclidean zero modes. Another argument in favor of local treatment of the CME is that in the Euclidean space the exact zero mode provides zero contribution to the electric currents and the electric charge density. This statement can readily be proven in the chiral basis of the Dirac matrices in which the γ matrices are 2×2-diagonal structures. Nevertheless, the topological charge fluctuations do induce the electric currents because in the presence of many positively and negatively charged lumps of topological charge (one can think of, e.g., an ensemble of instantons and anti-instantons) the zero modes split into very-near-zero modes. These near-zero modes carry information about the local topology of the lumps and create the electric currents. The low-lying modes do contribute to the electric quark's currents and this fact is clearly seen in our simulations.

Thus, in all our calculations we study the nonzero fermionic eigenmodes and we ignore the exact zero modes. Note that in large enough volumes the fermionic zero modes are suppressed and in the thermodynamic limit their contribution to certain physical observables—for example, to the chiral condensate [28] and to the chiral magnetization [18]—is zero. Indeed, as the volume increases the

number of the exact zero modes grows as the square root of the total volume while the number of the near-zero modes grows proportionally to the first power of the volume.

Finally, we mention that the space-time distribution and the dimensionality of the regions of space—where the left/right currents are imbalanced—may be as complicated as the distribution of the topological charge itself. The CME is expected to be realized due to the presence of the regions where the chiral density (11) of the former zero-modes (and now near-zero modes) of quarks is enhanced. We can probe the mechanism of the CME by investigation of the mutual correlations between the chiral density (11) and the electromagnetic current (12).

C. Electric charge density: An illustration

The basic feature of the CME is the spatial charge separation, which appears due to the presence of the nontrivial magnetic field B. The separation is a result of the existence of the quarks' electric current induced in the direction of the magnetic field. We call this current as the "longitudinal" electric current. According to our notations, the longitudinal direction is given by $\mu = 3$ for $T \neq 0$ and it covers the whole 03-plane for $T = 0$. The transverse (with respect to the magnetic field) components of the electric current belong to the 12-plane.

In order to illustrate the CME we have first studied a spatial excess of the charge density due to the presence of the magnetic field,

$$j_0(x; A, B) = \langle j_0(x)\rangle_{A,B} - \langle j_0(x)\rangle_{A,B=0}. \tag{14}$$

The subtraction in (14) removes all ultraviolet contributions leaving us with infrared nonperturbative contributions originating due to the external magnetic field.

Level surfaces of two typical charge density distributions in a fixed time slice of a zero-temperature gauge field configuration are shown in Figs. 1 and 2 for two values of the external magnetic field B.

We can deduce three interesting qualitative features from Figs. 1 and 2.

First, we notice that the external magnetic field indeed induces a spatial excess of the electric charge density. The stronger the field the larger the excess. This property is in agreement with our present understanding of the CME.

Second, the excess of the charge density is spatially extended along the direction of the magnetic field. This feature can be understood in terms of the standard electrodynamics [29]: the quarks are localized in the transverse plane with respect to the field as they tend to occupy low Landau levels (in Figs. 1 and 2 the transverse planes are horizontal). If there were no background gluon field then the longitudinal quark trajectories would not be affected by the field. In general quarks have a nonzero momentum in the longitudinal direction, so that the trajectories of the quarks should be elongated strictly in the direction of the magnetic field. The gluon background field provides a visible distortion to the quarks' motion. This feature is observed in both figures.

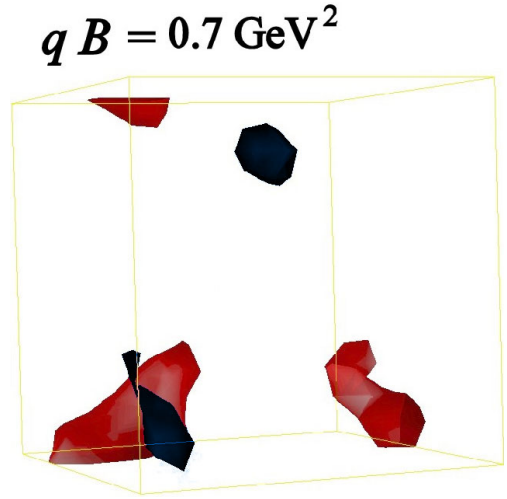

FIG. 1 (color online). The excess of the density of the electric charge (14) due to the applied magnetic field $qB = 0.7\ \mathrm{GeV}^2$ on 14^4 lattice with the volume $(1.44\ \mathrm{fm})^4$. A typical three-dimensional slice of a typical gauge field configuration is shown. The magnetic field is directed vertically from the bottom of the picture to the top. The red (gray) regions mark the excess of the positive charges while the blue (dark gray) regions correspond to the negative electric charge density.

Third, Figs. 1 and 2 illustrate a conceptual difficulty associated with identifying the electric dipole moment of the spatially separated charges in a finite volume. Because of the (periodic) boundary conditions the electric dipole moment is not a universal notion as it depends on the choice of the reference frame. Consider, for example, one-dimensional space of the finite length L with periodic boundary condition imposed. Two points separated by the distance $r > 0$ have the dipole moment $\mu_e = er > 0$.

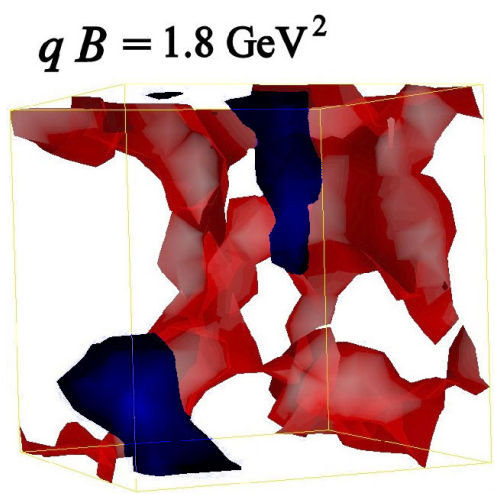

FIG. 2 (color online). The same as in Fig. 1 but for $qB = 1.8\ \mathrm{GeV}^2$ and for the configuration of non-Abelian gauge field.

However, if we change the direction of our reference frame, one can count the distance between the two points as $L - r$. As a consequence, we get the different value for the electric dipole moment $\mu_e = e(r - L) < 0$. The difference between the two definitions results in the large uncertainty of the electric dipole moment, and this fact makes the physical sense of the definition obscure. One can, of course, limit all distances on the lattice by $r \leq L/2$, so that if $r < L/2$, then we define $\mu_e = er$ while $r > L/2$ then $\mu_e = e(r - L)$. However, this definition is not satisfactory as well, because small variations of the charge around the most distant point $r \sim L/2$ lead to large variations of the electric dipole moment, $\mu_e \sim eL/2 \rightarrow -eL/2$. Another solution of this problem could be to replace the infinite-volume definition $\mu_e = er$ by its finite-volume counterpart, $\mu_e = ef(r, L)$, where the function f: (i) obeys the symmetry $f(r, L) = f(L - r, L)$ and (ii) reduces to $f \rightarrow r$ in the infinite volume limit, $L \rightarrow \infty$. However, this solution is not satisfactory either, because the electric dipole moments in intermediate volumes would inevitably be dependent on the form of chosen function $f(r, L)$.

Thus, the electric dipole moment is an ambiguous notion in finite volume. Therefore, instead of the electric dipole moments we study the electric currents. The induced currents represent a complimentary aspect of CME since the emergence of the electric dipole moment is necessarily associated with an electric current The advantage of the current-based approach is clear: the definition of the electric current (12) is a local notion which is not subjected—at least directly—to the finite volume ambiguities.

D. Chirality fluctuations and CME in cold matter

Since the CME originates due to fluctuations of the local chirality, we first study the effect of the external magnetic field on the expectation value of the square of the local chirality (11):

$$\langle \rho_5^2 \rangle_{IR}(B, T) = \frac{1}{V} \int_V d^4x \langle \rho_5(x)\rho_5(x) \rangle_{B,T} - \frac{1}{V} \times \int_V d^4x \langle \rho_5(x)\rho_5(x) \rangle_{B=0,T=0}. \quad (15)$$

Here V is the total volume of the lattice, and $\langle \ldots \rangle_{B,T}$ means expectation value with respect to the thermal state at temperature T with background magnetic field B. Subtraction of the expectation value at zero temperature ($T = 0$) and in the absence of the external field ($B = 0$) removes all ultraviolet divergences providing us with a physical quantity which should be insensitive to the ultraviolet cutoff. In fact, the quantity (15) provides us with the strength of the chirality fluctuations because in the equilibrium QCD the average of the chirality is zero, $\langle \rho_5 \rangle = 0$. We denote the result of the subtraction by the subscript "IR" in $\langle \ldots \rangle_{IR}$ stressing the importance of the nonperturbative infrared (IR) contributions. In all our expectation values the corresponding zero-temperature and zero-field contributions are always subtracted as it is done in (15). Note that the coordinates of all operators entering our observables, including Eq. (15), are taken at one point x.

Because of the subtraction, the expression (15) gives us the influence of the magnetic field and/or finite temperature on the strength of the chirality fluctuations. We plot this quantity in Fig. 3 for a few values of the lattice spacing a, lattice volumes L^4, and the number of low eigenmodes M which are used to calculate the Dirac propagator (8). We found that the variations of all these parameters change the expectation values by less than 10%, thus confirming good scaling of our results.

The CME appears due to the local topology of the gauge field configurations. The topological content of the gauge field configurations is reflected in the structure of the exactly-zero and near-zero eigenmodes. The exactly zero eigenmodes are not significant in the Euclidean space as we have discussed above. However, the near-zero modes play an important role in the CME, and they also come with larger weights in the propagator (8). Thus, the consideration of only low-lying zero modes is justified. For our particular observables, the errors associated with our truncation scheme are smaller than the typical statistical errors. However, we should make a cautionary remark that as the volume of the lattice increases, the density of low-lying eigenmodes grows, and one should take into account more and more of them.

Notice that most of figures in our paper are plotted in the logarithmic scale, and that for dimensional reasons the data for chirality fluctuations and, later, for current fluctuations are always expressed in GeV^6. Because of the high (sixth) power the actual values of our quantities look quite small, but this fact in no way indicates that the physical effects are

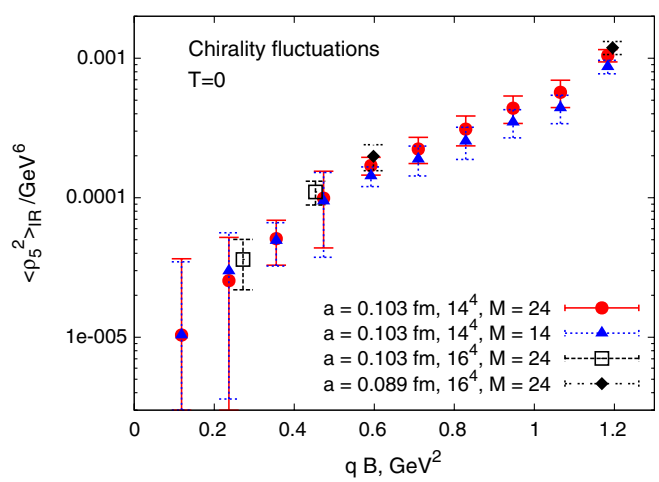

FIG. 3 (color online). The expectation value of the chirality squared (15) ρ_5^2 vs magnetic field at different lattice parameters (the lattice spacing a and the lattice volume L^4), and for different number M of Dirac eigenmodes which were taken to determine the truncated Dirac propagator (8) used in (3) to calculate (15).

small. For example, in Fig. 3 at $qB = 1.5$ GeV^2 the value of the chirality fluctuation is $\langle\rho_5^2\rangle = 10^{-4}$ GeV^6. This number corresponds to the large quantity $\langle\rho_5^2\rangle \approx (215\ \text{MeV})^6$ if the magnitude is expressed in terms of MeV.

In Fig. 4 we show the dependence of the expectation value $\langle\rho_5^2\rangle_{IR}(B, T)$ on the magnetic field at three temperatures: at zero temperature, at finite temperatures in the confinement phase ($T = 0.82T_c$), and in the deconfinement phase just above the phase transition, $T = 1.12T_c$. At zero temperature the fluctuations of the chirality quickly grow with magnetic field. As the temperature increases the growth rate gets smaller and in the deconfinement phase the chirality fluctuations are almost insensitive to the value of the magnetic field.

In the absence of the external magnetic field, $B = 0$, the rise of temperature leads, according to Fig. 4, to the increase of the chirality fluctuations. However, sufficiently strong magnetic fields can also induce the enhancement effect comparable to the effect of the thermal fluctuations. For example, the chirality fluctuations at zero temperature in the magnetic field of the strength $qB \sim 2$ GeV^2 has the same value as the fluctuations of chirality in the absence of the external magnetic field at temperature $T = 1.12T_c$:

$$\langle\rho_5^2(x)\rangle_{T=0,B=2\ \text{GeV}^2} \approx \langle\rho_5^2(x)\rangle_{T=1.12T_c,B=0}. \tag{16}$$

It is known that the temperature suppresses the fluctuations of the *global* topological charge [30],

$$\chi_Q = \frac{1}{V}\langle Q^2\rangle. \tag{17}$$

Lattice studies show that in Yang-Mills theory the fluctuations are almost independent of the temperature in the confinement phase,

$$\chi_Q(T = T_c) \approx \chi_Q(T = 0),$$

while as temperature exceeds the critical point, $T > T_c$, the fluctuations vanish quickly [31]. For example, in $SU(2)$ Yang-Mills theory just above the phase transition, $T = 1.1T_c$, the value of the fluctuations is more than twice smaller compared to the value in the confinement phase [31],

$$\chi_Q(T = 1.1T_c) \approx 0.5\chi_Q(T = T_c).$$

Moreover, it is clear that in quenched theory the topological charge of the gluon fields is not affected by the external magnetic field, because the coupling between gluons and electromagnetism is provided by the dynamical quarks which are absent in the quenched theory. These observations suggest that the *local* fluctuations of the chirality (15) and the fluctuations of the *global* topological charge (17) are not related directly. It is more likely that at high temperatures chirality-changing transitions occur due to local processes involving sphaleronlike configurations [32]. At zero temperature one might explain chirality changes as follows: in a strong magnetic field, a quark undergoes one-dimensional motion along the magnetic field. Quark chirality can be efficiently changed in local one-dimensional scattering processes on the fluctuations of gauge fields, where the spin is not affected but the momentum changes its sign. In the deconfinement phase this mechanism does not work because the influence of the gluon fluctuations on the quark's motion is lower in this phase (the quark confinement is lost, for example) and one can suggest that the typical scattering does not reflect the momenta.

Concluding this subsection, we notice that the CME crucially depends on the imbalance between the left and right chiral modes. The local strength of the chiral imbalance is characterized by the value of the chirality fluctuations, $\langle\rho_5^2\rangle$, which determines the rate of chirality-changing transitions. Since the external magnetic field strongly enhances the chirality fluctuations (they become comparable with the fluctuations in the deconfinement phase) so that the chiral magnetic effect—if we imagine for a moment that the property of the color confinement were either absent or inessential due to density effects—could be observed in cold nuclear matter as well.

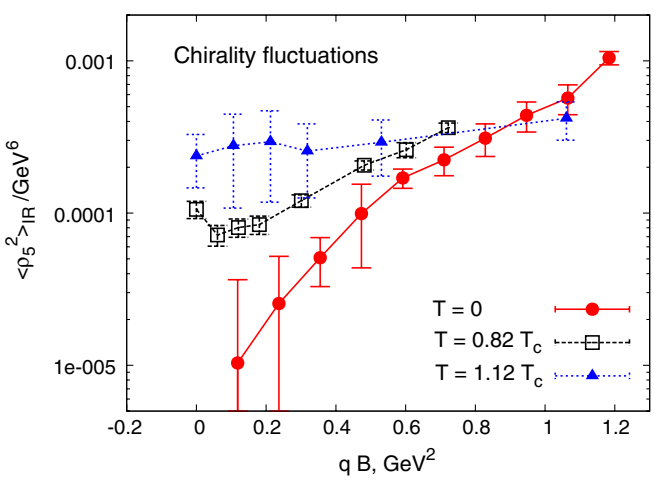

FIG. 4 (color online). The expectation values of the chirality squared (15) vs the magnetic field at three different temperatures.

E. Fluctuations of electromagnetic current

We checked that the expectation value of all components of the electromagnetic current itself (14) is zero within the error bars. This fact is not unexpected because the magnetic field passes through the regions of space-time characterized by positive and negative chiralities (11). According to the CME, in regions with opposite chiralities the magnetic field induces the electric currents in opposite directions with respect to the magnetic field. Thus, globally, the longitudinal electric currents should cancel each other. As for the transverse (with respect to the magnetic field) spatial directions, the electric currents should cancel each other because of circular motion on (perturbed)

Landau levels. Finally, the average timelike current is zero because of the Gauss theorem (the total electric charge in a closed volume with periodic boundary conditions should be zero). These statements are valid both at zero and at nonzero temperatures.

Below we study the dispersion of the electromagnetic current

$$\langle j_\mu^2\rangle_{IR}(B,T) = \frac{1}{V}\int_V d^4x\langle j_\mu^2(x)\rangle_{B,T} - \frac{1}{V} \times \int_V d^4x\langle j_\mu^2(x)\rangle_{B=0,T=0} \quad [\text{no sum over } \mu], \tag{18}$$

instead of the expectation value of the electric current. Note that here and below no sum over the Lorenz index μ is assumed in all our expressions involving j_μ^2.

Following study of the fluctuations of chirality, we first check that the internal lattice parameters do not influence the final results (the fluctuations of the electromagnetic current calculated are shown at different lattice parameters in Fig. 5). Then in Fig. 6 we plot the expectation values of the fluctuations of each component of the electric current at zero temperature. At $T = 0$ the rotational symmetry is broken only by the electromagnetic field strength tensor $F_{\mu\nu}$ with $F_{12} \neq 0$, so that the components of the electric currents can be grouped into transverse and longitudinal sets, respectively,

$$\langle j_1^2\rangle = \langle j_2^2\rangle, \qquad \langle j_0^2\rangle = \langle j_3^2\rangle \qquad (T = 0). \tag{19}$$

At weak magnetic fields all components have the fluctuations of the same order. However, at stronger fields the fluctuations of the longitudinal currents (j_3 and j_0) are stronger compared to the fluctuations the transverse currents (j_1 and j_2). Both transverse and longitudinal components grow with the magnetic field, but the longitudinal components grow faster. Thus we see that at zero temperature the magnetic field enhances both the current j_3 in the direction of the magnetic field and the charge density j_0, which is a clear signature of the charge separation associated with the CME. The enhancement of the transverse components j_1 and j_2 in the magnetic field is natural since the transverse momentum of a particle occupying a Landau level grows with the increase of the magnetic field.

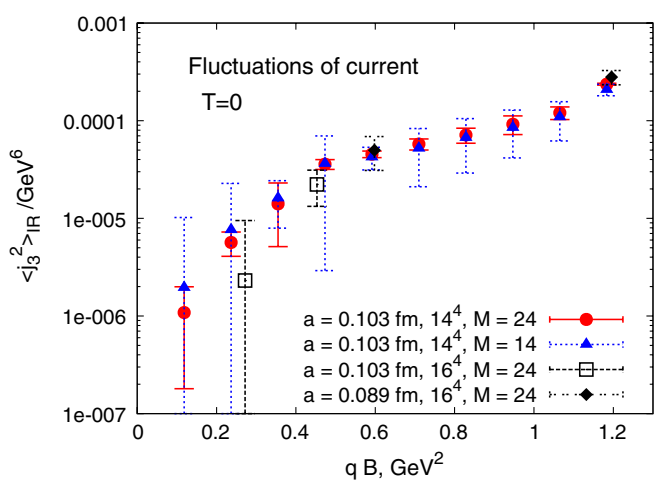

FIG. 5 (color online). The same as in Fig. 3 but for the fluctuations (18) of the electromagnetic current j_3 (12).

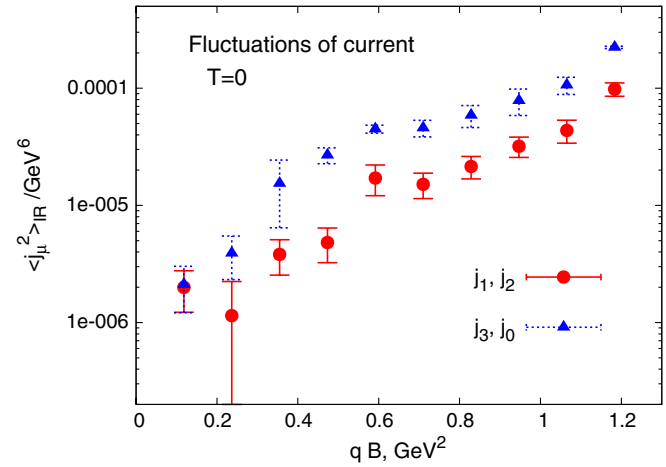

FIG. 6 (color online). The expectation value of the squares of the transverse (j_1, j_2) and longitudinal (j_3, j_0) components of the vector current (12) vs the applied magnetic field at zero temperature.

At nonzero temperature the (discrete) rotational symmetry is broken not only by the electromagnetic field, $F_{12} \neq 0$, but also by the compactified temperature direction $\mu = 0$. Therefore the charge fluctuations ($\mu = 0$) lose the similarity with longitudinal ($\mu = 3$) current fluctuations, while the fluctuations of the transverse ($\mu = 1, 2$) currents are still degenerate,

$$\langle j_1^2\rangle = \langle j_2^2\rangle, \qquad \langle j_0^2\rangle \neq \langle j_3^2\rangle \qquad (T \neq 0). \tag{20}$$

In Fig. 7 we plot the fluctuations of all components of the electric currents at finite temperature $T = 0.82T_c$, at which the system is still in the confinement phase. One can see that at zero magnetic field the currents fluctuate strongly due to thermal fluctuations. All components of the electric currents fluctuate approximately with the same strength. As the magnetic field grows the fluctuations of all components drop a bit, and then they start to grow steadily. The growth rate is noticeably smaller compared to the slope observed at zero temperature, Fig. 6. On the other hand, there are similarities with the zero-temperature case: (i) the fluctuations of the charge density and of the longitudinal (with respect to the magnetic field) current have equal magnitudes; and (ii) the longitudinal currents fluctuate stronger compared to the transverse currents.

The situation turns out to be quite different in the deconfinement phase, Fig. 8. First, the fluctuations of the longitudinal current are insensitive to the strength of the magnetic field. Second, both the charge and transverse current fluctuations are decreasing functions of the field

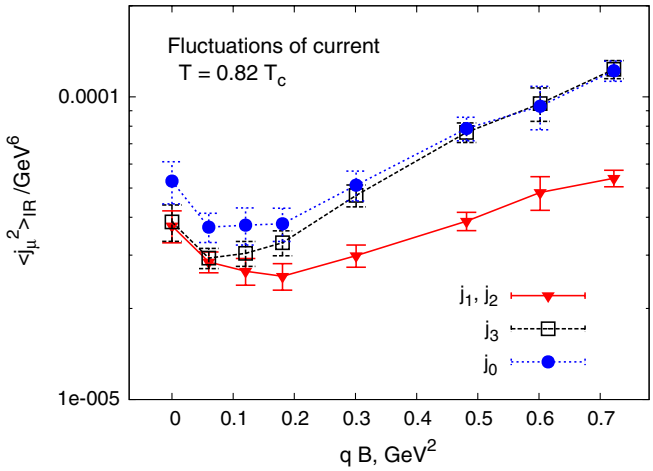

FIG. 7 (color online). The same as in Fig. 6 but for $T = 0.82T_c$. The longitudinal components j_3 and j_0 differ due to nonzero temperature (20).

strength. The drop in the electric charge fluctuations is especially noticeable. This feature can be explained by an effect of the thermal Debye screening [33].

In Fig. 9 we show the ratio of the longitudinal component of the current to its transverse component. At zero temperature the current is substantially enhanced at $qB \sim 1.5\ \mathrm{GeV}^2$, while at relatively weak fields, $qB \sim 0.3\ \mathrm{GeV}^2$, the enhancement of the current is not seen.

At nonzero temperature the relative enhancement is weaker. The ratios at $T = 0.82T_c$ and at $T = 1.12T_c$ have similar properties which are in qualitative agreement with the CME features: at low magnetic fields the longitudinal and transverse directions are equivalent and the increase of the magnetic field gives a bit stronger preference for the longitudinal direction with respect to the transverse one.

We have already mentioned the reasons why the CME is expected to exist in the high temperature phase [1], where

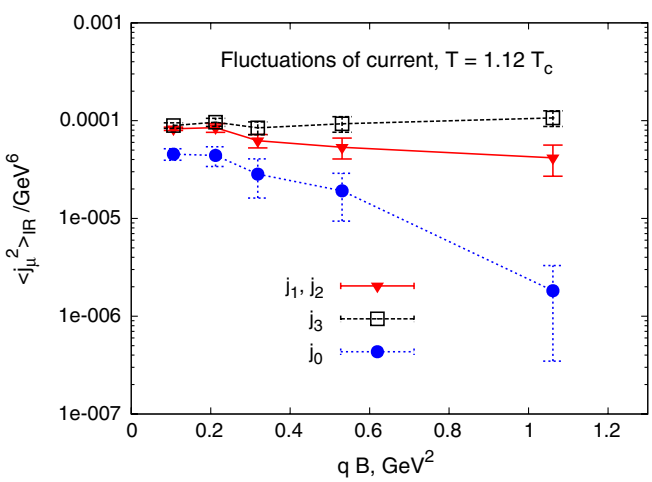

FIG. 8 (color online). The same as in Fig. 7 but for $T = 1.12T_c$.

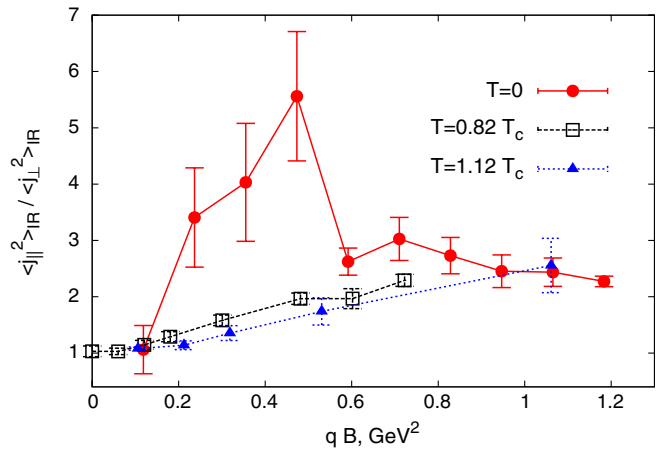

FIG. 9 (color online). The ratio of the longitudinal current to the transverse one vs the strength of the magnetic field at various temperatures.

the confinement is absent and the chiral symmetry is restored. The reasons are quite simple: the presence of the chiral condensate destroys imbalance between the right and left chiral modes while the confinement does not allow the spatial separation of the quarks at distances larger than the confinement distance. This argument seems to be independent of the inclusion of the dynamical (virtual) quarks into the consideration, so that it should be valid, in lattice language, both in quenched and in unquenched theories.

We have found that in the quenched approximation the qualitative signatures of the chiral magnetic effect exist both in the confinement and in the deconfinement phases. In all our simulations, at zero temperature and at finite temperature above and below the critical point, we see that the longitudinal component of the electric (vector) current dominates over the transverse component. However, in the confinement phase the electric current rises as the function of the external magnetic field while in the deconfinement phase the value of the current is almost insensitive to the strength of the magnetic field.

F. Chirality-current correlations

According to the CME the longitudinal electric current may locally be induced by the imbalance of chirality. Therefore it is natural to expect that the local fluctuations of the longitudinal electric currents are correlated with the chirality fluctuations. However, the correlator of the chirality and the electric current $\langle \rho_5 j_\mu \rangle$ vanishes, since in isotropic homogeneous space it is impossible to construct an axial vector from an antisymmetric tensor of magnetic field strength. Therefore, we have considered the correlation between the squares of the induced current and the chirality:

$$c(\rho_5^2, j_\mu^2) = \frac{\langle \rho_5^2 j_\mu^2 \rangle - \langle \rho_5^2 \rangle \langle j_\mu^2 \rangle}{\langle \rho_5^2 \rangle \langle j_\mu^2 \rangle}. \tag{21}$$

It turns out that in the confinement phase the corresponding correlation functions for all components of the electric currents vanish within statistical uncertainty,

$$c(\rho_5^2, j_\mu^2) \simeq 0 \qquad T \lesssim T_c. \tag{22}$$

In the deconfinement phase the correlation function (21) is not zero (Fig. 10), while the correlation decreases with the increase of the magnetic field. All these facts suggest that the enhancement of the fluctuations of current in the direction of the magnetic field is not locally correlated with the chirality fluctuations.

We would like to emphasize that the absence of the local correlation does not in general mean the independence of the longitudinal currents on the chiral density. The longitudinal current can be caused by the chirality fluctuations and, at the same time, the current itself may be not localized in the local regions of the space-time where the chiral density is enhanced. Although this statement sounds puzzling, similar effects are already known in the condensed matter physics. For example, the well-known Anderson localization [34] of electrons inside a semiconductor is caused by the presence of impurities. However, the spatial regions, in which the electron wave functions are localized, do not coincide with the positions of the impurities themselves.

G. Clean case: Instantonlike configuration

In the previous sections we have studied the CME using the gluon fields of the quantum vacuum. Such gluonic fields contain ultraviolet fluctuations both of perturbative and nonperturbative nature. In particular, the topological charge density is subjected to strong fluctuations with quite nontrivial localization properties, so that the CME should be realized locally in a vicinity of each topological lump. In order to illustrate the existence of the CME in a more theoretical fashion, we have prepared a smooth instanton-like gluon field with a unit topological charge on the lattice 14^4 and applied the external magnetic field to this configuration. In Fig. 11 we show the behavior of the chirality fluctuations and the fluctuations of longitudinal electric current at this instantonlike background.

The first indication of the existence of the CME comes from the observation of the increase of chirality fluctuations with increases of the strength of the external magnetic field. Figure 11 illustrates that the external magnetic field, on average, enhances a local imbalance between approximately left and approximately right fermionic modes in the background of this $Q = 1$ configuration. The effect may readily be understood as a consequence of the CME: the magnetic fields tend to localize "left" and "right" fermionic modes in different parts of the space-time because the left and right modes have opposite magnetic moments. The external magnetic field acts as a chemical potential which provides a different weight to these modes. The left and right modes have opposite direction of the momentum with respect to the magnetic moment so that the external magnetic field tries to separate them spatially as well. Thus, the positive and negative chiralities do not compensate themselves in ρ_5, leading to increase of the chirality fluctuations.

The second signature in favor of the CME appears in the properties of the (squared) longitudinal electric current. Notice that the longitudinal current contains, in fact, contribution from the two components, j_3 and j_0, because they are indistinguishable from a geometrical point of view (we remind that we are working at zero temperature in external magnetic field $B = F_{12}$). Therefore we also plot in Fig. 11 the absolute value of the longitudinal current squared, $j_\parallel^2 = j_0^2 + j_3^2$ which turns out to be an increasing function of the magnetic field. This behavior is consistent with our understanding of the CME.

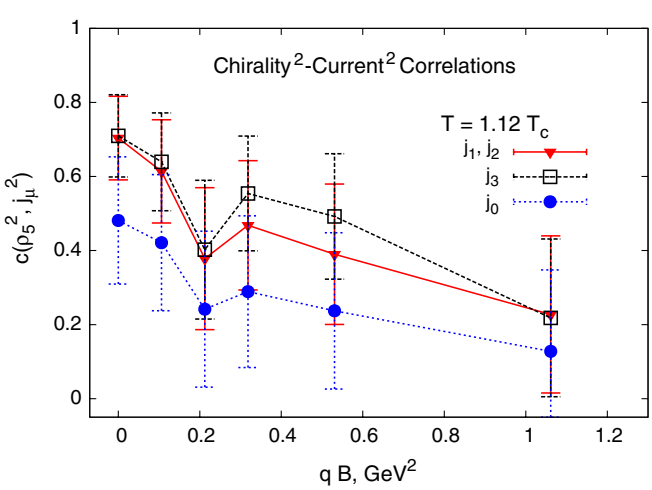

FIG. 10 (color online). The correlation between squared chirality and squared electric current (21).

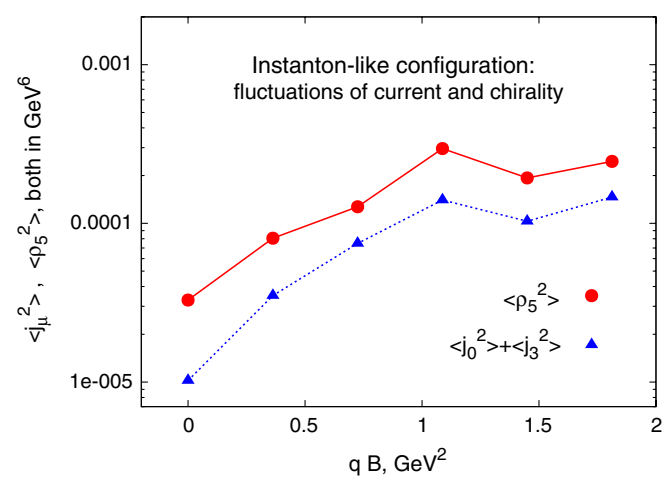

FIG. 11 (color online). The fluctuations of the chirality (15) and the fluctuations of the longitudinal electric current (18) at an instantonlike configuration with unit topological charge as a function of the applied magnetic field.

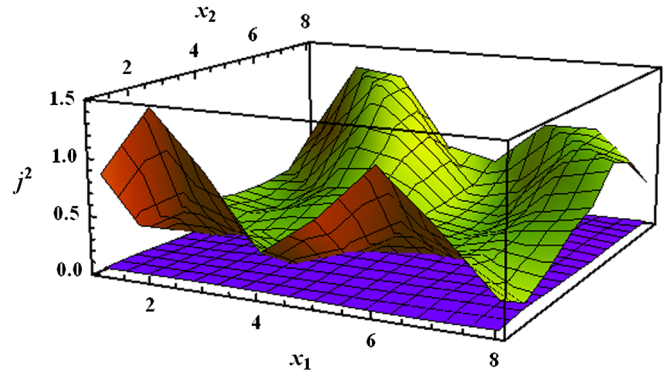

FIG. 12 (color online). The squared components of the electric current (in arbitrary units) in a 12-plane on the background of an instantonlike configuration with topological charge $Q = 1$. The upper (green) sheet represents the spatial distribution of the longitudinal current $j_\parallel^2 = j_0^2 + j_3^2$, and the lower (violet) sheet corresponds to the transverse current $j_\perp^2 = j_1^2 + j_2^2$.

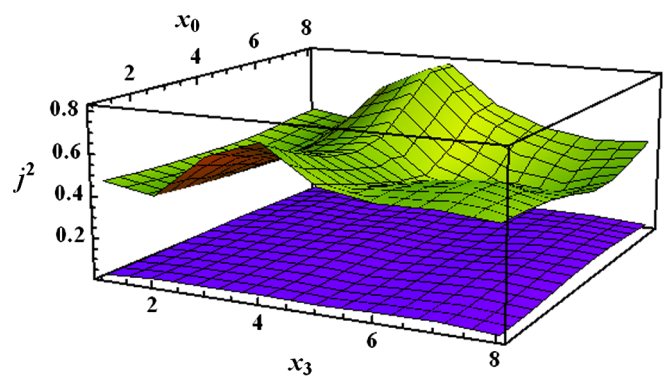

FIG. 13 (color online). The same as in Fig. 12 but for a 03-plane of the same gluon field.

In order to provide an illustration of the effect, we visualize the squared transverse and longitudinal electric current densities for the $Q = 1$ configuration in the external magnetic field. In Figs. 12 and 13 we show the current densities in the 12 and 34 cross sections, respectively. One can clearly see that in a strong magnetic field the longitudinal component is always larger than the transverse one in agreement with the prediction of the CME.

Concluding this subsection we summarize that our study of an instantonlike configuration of the gluonic field with the topological charge $Q = 1$ supports the existence of the chiral magnetic effect.

III. CHARGE ASYMMETRY: COMPARISON WITH EXPERIMENT

Experimental signatures of the chiral magnetic effect are usually discussed in terms of the following observables, suggested first in Ref. [7]:

$$a_{ab} = \frac{1}{N_e}\sum_{e=1}^{N_e}\frac{1}{N_a N_b}\sum_{i=1}^{N_a}\sum_{j=1}^{N_b}\cos(\phi_{ia} + \phi_{jb}), \tag{23}$$

where $a, b = \pm$ labels positively/negatively charged particles, N_e is the total number of experimental events, N_a and N_b are the numbers of positively/negatively charged particles produced in each event, and ϕ_{ia}, ϕ_{jb} are the azimuthal angles of the momenta of the produced particles with respect to the reaction plane.

These observables can be expressed in terms of the total charge separated in each event as [1]

$$a_{ab} = \frac{c\langle\Delta_a\Delta_b\rangle}{\langle N_a\rangle\langle N_b\rangle}, \tag{24}$$

where $a, b = \pm$, Δ_+ is the difference of the total numbers of positively charged particles emitted above or below the reaction plane, Δ_- is the same quantity for negatively charged particles, and c is some coefficient (of order of unity) which depends on the characteristics of the hydrodynamical flow in the reaction. One also has $\langle N_a\rangle = \langle N_b\rangle = N_q$, where the average total number of the particles of the same charge per event N_q (for Au-Au collisions) can be found, e.g., in Table 1 in [1].

In order to compare experimental data with our results, it is convenient to consider the following combination of a_{ab}:

$$a_{++} + a_{--} - 2a_{+-} = \frac{\langle(\Delta Q)^2\rangle}{N_q^2} = \frac{\langle(\Delta_+ - \Delta_-)^2\rangle}{N_q^2}, \tag{25}$$

where $\Delta Q = \Delta_+ - \Delta_-$ is the difference of total charges of particles emitted above and below the reaction plane. $\langle(\Delta Q)^2\rangle$ can be estimated from our lattice data on $\langle j_\mu^2\rangle$ using the following rough model: consider a fireball of radius R created during the heavy-ion collision, and assume that it emits positively or negatively charged particles from each element of surface $\delta\vec{\sigma}_i$, with $|\delta\vec{\sigma}_i| \sim \rho^2$. The quantity ρ is some characteristic correlation length, so that emission of particles on each surface element of the area ρ^2 is statistically independent. ΔQ is calculated as the difference of the total charges emitted in some characteristic collision time τ from the upper and from the lower hemispheres of the surface of the fireball:

$$\delta Q = \tau\sum_i \mathrm{sign}(\delta\vec{\sigma}_i\cdot\vec{B})\vec{j}_i\cdot\delta\vec{\sigma}_i. \tag{26}$$

For the expectation value $\langle(\Delta Q)^2\rangle$ one then has

$$\begin{aligned}\langle(\Delta Q)^2\rangle &= \tau^2\sum_i\langle(\vec{j}_i\cdot\delta\vec{\sigma}_i)^2\rangle \\ &= \tau^2\rho^2\sum_i\langle(\vec{j}_i\cdot n_i)^2\rangle|\delta\vec{\sigma}_i| = \tau^2\rho^2\int d\vec{n}\langle\vec{j}\cdot\vec{n}\rangle^2.\end{aligned} \tag{27}$$

We further assume that emission in different directions is independent: $\langle j_\mu j_\nu\rangle = 0$ for $\mu \neq \nu$. With these assump-

tions, we finally arrive at the following expression for $\langle(\Delta Q)^2\rangle$:

$$\frac{\langle(\Delta Q)^2\rangle}{N_q^2} = \frac{4\pi\tau^2\rho^2R^2}{3N_q^2}(\langle j_\parallel^2\rangle + 2\langle j_\perp^2\rangle), \tag{28}$$

where $j_\parallel$ and $j_\perp$ are, respectively, the currents along the magnetic field and perpendicular to it. We take the values of N_q from Table 1 in [1] and use our lattice data on $\langle j_\parallel^2\rangle$ and $\langle j_\perp^2\rangle$ at $T = 1.12T_c$. Here we take into account the fact that the expectation value of the squared spatial currents in the Minkowski and Euclidean spaces are the same.

In Table 1 in [1] one can also find a relation between centrality ("% most central") and the ratio b/R, where b is the impact parameter. From expression (A.12) in [1] one can roughly estimate the magnetic field during the collision as $eB \sim (0.1b/R)$ GeV^2. For simplicity, we assume that the magnetic field is nonzero and constant only during the time τ. In order to obtain $\langle(\Delta Q)^2\rangle$ at small values of magnetic field we have used polynomial interpolation. The resulting plot is shown in Fig. 14. Experimental points obtained by the STAR Collaboration are taken from the plots presented in [8,9]. The coefficient $\tau^2\rho^2R^2$ in (28) was fitted so that the lattice data and the theoretical data match best. One can take, for example, $\tau \sim 1$ fm, $R \sim 5$ fm, $\rho \sim 0.2$ fm, which are reasonable values by order of magnitude, especially for such a rough model.

We observe a good agreement between our data and the experimental results. *Despite the agreement seen at the quantitative level, the approximations used in our lattice technique suggest that this result should be considered as a qualitative indication rather than a solid proof.* It should be noted that at $T = 1.12T_c$ the dependence of $\langle j^2\rangle$ and hence of $\langle(\Delta Q)^2\rangle$ on the magnetic field is rather weak, and, moreover, the current does not increase with magnetic field. We have to conclude that the dominant effect which determines the shape of the plot on Fig. 14 is the decrease of N_q with centrality (see Table 1 in [1]). It could be therefore much more informative to consider the observables b_{ab} introduced in [1], which do not contain the normalization factors $\frac{1}{N_aN_b}$. These observables can be directly compared with our data for the observable $\langle j_\mu^2\rangle$, both in the deconfinement phase and at zero temperature. Note also that since at zero temperature the current increases with magnetic field much faster than at high temperature, it might be not unreasonable to search for strong magnetic effects also in cold (and dense) nuclear matter.

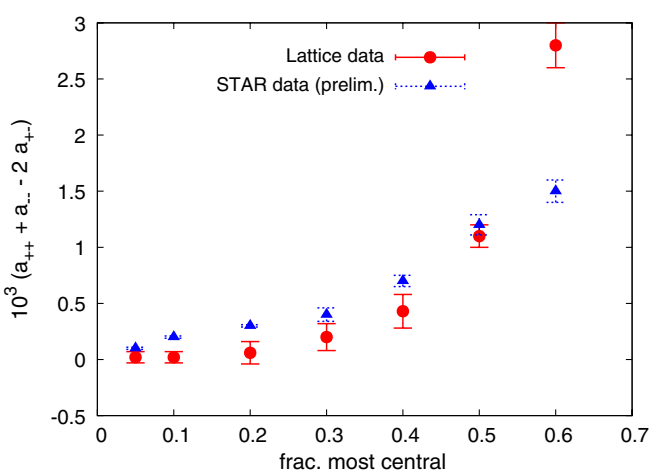

FIG. 14 (color online). The average fluctuations of the difference of total electric charges of particles emitted above and below the reaction plane: comparison of the experimental observable of [8,9] (the filled triangles) with our lattice data (the filled circles).

IV. CONCLUSIONS

In this paper we studied possible signatures of the chiral magnetic effect [1,4–6] in quenched $SU(2)$ lattice gauge theory using the chirally invariant Dirac operator. We observed the expected enhancement of the electric current in the direction of the magnetic field both in quantum configurations of the gluon fields and in a fixed instantonlike gauge field with nonzero topological charge. The CME at the instantonlike configurations is much more pronounced compared to the real gluonic vacuum (an illustration can be found in Figs. 12 and 13). The CME is based on the imbalance between left and right fermionic modes. The measure of the local imbalance is the chiral density of the quarks. On average the global chiral charge is zero, while the local fluctuations of the chiral density can be quite strong. We found (Fig. 4) that at zero temperature the chiral fluctuations are drastically enhanced (by 2 orders of magnitude) in the applied magnetic field.

As the temperature increases the chirality fluctuations increase and, simultaneously, they become less sensitive to the strength of the magnetic field. In the deconfinement phase the local chirality fluctuates much stronger compared to the fluctuations at zero temperature while the fluctuations themselves are practically independent of the strength of the magnetic field. The enhancement of the chirality fluctuations due to magnetic field can be illustrated by the following example: in strong magnetic field $qB = 2.5$ GeV^2 at zero temperature $T = 0$ the chirality fluctuations take the same value $\langle\rho_5^2\rangle \approx (220\ \text{MeV})^6$ as in the case of zero magnetic field $qB = 0$ and high temperature $T = 1.12T_c$.

In the confinement and in the deconfinement phases the properties of the induced electric currents differ strongly. At zero temperature the longitudinal (i.e., directed along the magnetic field) currents grow with the increase of the strength of the magnetic field. This effect is accompanied by a (weaker) enhancement of the transverse currents, which we attribute to a transverse squeezing of the Landau levels (Fig. 6).

At nonzero temperature but still below the transition $T = 0.82T_c$, the slopes of enhancement of both longitudinal and transverse electric currents become smaller.

However, the longitudinal current is enhanced stronger than the transverse current (Fig. 7).

In the deconfinement phase at $T = 1.12T_c$ the fluctuations of the longitudinal currents are almost independent of the magnetic field. Moreover, the transverse components of the electric current decrease slightly as the magnetic field gets stronger. The fluctuations of the electric charge density become drastically suppressed in the deconfinement phase in the strong enough magnetic field (Fig. 8).

We also found that the presence of a nonzero *global* topological charge in the real gluonic configurations leads to a little effect on the longitudinal currents. This happens because the influence of a global charge is largely overshadowed by strong *local* fluctuations of the topological charge. We conclude that in our simulations the CME is realized at local lumps of topological charge in the gluonic configuration.

We would like to make here a cautionary notice that our investigation utilized many approximations. We used two colors instead of three, our simulations are done in the quenched approximation, the fermionic propagators were truncated, and the system was studied in a finite volume. We found that the systematic errors associated with truncation, finite-size and finite-volume effects are smaller than our statistical errors, and we expect on general grounds that the reduced number of colors should not affect our results drastically. However the absence of the dynamical fermions may in general correct our results. We got a qualitative indication of the existence of the CME, while the quantitative features of the CME may be accessible only in simulations with dynamical quarks.

Finally, in real heavy-ion collisions the magnetic field is perpendicular to the reaction plane. Consequently, the CME implies an imbalance between total electric charge observed above and below the reaction plane which is indeed seen in preliminary data published by the STAR Collaboration at RHIC [8,9]. Using a simple model of a fireball we obtain a good agreement between our data and experimental results of the STAR Collaboration (Fig. 14) on the average fluctuations of the difference of total charges of particles emitted above and below the reaction plane.

ACKNOWLEDGMENTS

The authors are grateful to V. G. Bornyakov, A. S. Gorsky, B. O. Kerbikov, D. Kharzeev, S. M. Morozov, M. Müller-Preussker, V. A. Novikov, M. I. Vysotsky, H. Warringa, and V. I. Zakharov for interesting discussions. This work was partly supported by RFBR Grant Nos. 08-02-00661-a, 06-02-17012, DFG-RFBR 436 RUS, and BRFBR F08D-005; a grant for scientific schools No. NSh-679.2008.2; by the Federal Program of the Russian Ministry of Industry, Science and Technology No. 40.052.1.1.1112; and by the Russian Federal Agency for Nuclear Power. P. V. Buividovich is also supported by the DAAD and by the Dynasty Foundation. The calculations were partially done on the MVS 50K at Moscow Joint Supercomputer Center.

[1] D. E. Kharzeev, L. D. McLerran, and H. J. Warringa, Nucl. Phys. **A803**, 227 (2008).
[2] B. C. Tiburzi, Nucl. Phys. **A814**, 74 (2008).
[3] N. O. Agasian and S. M. Fedorov, Phys. Lett. B **663**, 445 (2008); E. S. Fraga and A. J. Mizher, Phys. Rev. D **78**, 025016 (2008); Nucl. Phys. **A820**, 103c (2009).
[4] K. Fukushima, D. E. Kharzeev, and H. J. Warringa, Phys. Rev. D **78**, 074033 (2008); H. J. Warringa, arXiv:0906.2803; D. E. Kharzeev, arXiv:0906.2808.
[5] D. Kharzeev, R. D. Pisarski, and M. H. G. Tytgat, Phys. Rev. Lett. **81**, 512 (1998).
[6] D. Kharzeev, Phys. Lett. B **633**, 260 (2006).
[7] S. A. Voloshin, Phys. Rev. C **70**, 057901 (2004).
[8] S. A. Voloshin (STAR Collaboration), arXiv:0806.0029.
[9] H. Caines (STAR Collaboration), arXiv:0906.0305.
[10] E. Witten, Nucl. Phys. **B156**, 269 (1979).
[11] G. Veneziano, Nucl. Phys. **B159**, 213 (1979).
[12] L. D. McLerran, E. Mottola, and M. E. Shaposhnikov, Phys. Rev. D **43**, 2027 (1991).
[13] H. B. Nielsen and M. Ninomiya, Phys. Lett. **130B**, 389 (1983).
[14] M. A. Metlitski and A. R. Zhitnitsky, Phys. Rev. D **72**, 045011 (2005).
[15] G. 't Hooft, Phys. Rev. D **14**, 3432 (1976); **18**, 2199(E) (1978).
[16] A. I. Vainshtein, V. I. Zakharov, V. A. Novikov, and M. A. Shifman, Usp. Fiz. Nauk **136**, 553 (1982) [Sov. Phys. Usp. **25**, 195 (1982)].
[17] P. V. Buividovich, M. N. Chernodub, E. V. Luschevskaya, and M. I. Polikarpov, arXiv:0812.1740.
[18] P. V. Buividovich, M. N. Chernodub, E. V. Luschevskaya, and M. I. Polikarpov, arXiv:0906.0488.
[19] V. G. Bornyakov, E. V. Luschevskaya, S. M. Morozov, M. I. Polikarpov, E. M. Ilgenfritz, and M. Muller-Preussker, Phys. Rev. D **79**, 054505 (2009).
[20] V. G. Bornyakov, E. M. Ilgenfritz, B. V. Martemyanov, S. M. Morozov, M. Muller-Preussker, and A. I. Veselov, Phys. Rev. D **76**, 054505 (2007).
[21] C. Aubin, K. Orginos, V. Pascalutsa, and M. Vanderhaeghen, arXiv:0809.1629.
[22] F. X. Lee, R. Kelly, L. Zhou, and W. Wilcox, Phys. Lett. B **627**, 71 (2005).
[23] R. J. Crewther, Phys. Lett. B **70**, 349 (1977).
[24] H. Neuberger, Phys. Lett. B **417**, 141 (1998).
[25] M. H. Al-Hashimi and U. J. Wiese, Ann. Phys. (N.Y.) **324**, 343 (2009).

[26] I. Horvath *et al.*, Phys. Rev. D **68**, 114505 (2003); Y. Koma, E. M. Ilgenfritz, K. Koller, G. Schierholz, T. Streuer, and V. Weinberg, Proc. Sci. LAT2005 (2006) 300; C. Aubin *et al.* (MILC Collaboration), Nucl. Phys. B, Proc. Suppl. **140**, 626 (2005); V. I. Zakharov, Phys. At. Nucl. **68**, 573 (2005); F. V. Gubarev, S. M. Morozov, M. I. Polikarpov, and V. I. Zakharov, JETP Lett. **82**, 343 (2005); A. V. Kovalenko, S. M. Morozov, M. I. Polikarpov, and V. I. Zakharov, Phys. Lett. B **648**, 383 (2007); E. M. Ilgenfritz, K. Koller, Y. Koma, G. Schierholz, T. Streuer, and V. Weinberg, Phys. Rev. D **76**, 034506 (2007).

[27] Note that the words ''exact and Euclidean'' are very important here. The exact zero modes in the Minkowski space or, as we will see below, the near-zero modes in the Euclidean space are important for the CME.

[28] T. Banks and A. Casher, Nucl. Phys. **B169**, 103 (1980).

[29] L. D. Landau and E. M. Lifshitz, *Quantum Mechanics: Non-Relativistic Theory*, Course of Theoretical Physics Vol. 3 (Pergamon, New York, 1980).

[30] R. D. Pisarski and L. G. Yaffe, Phys. Lett. **97B**, 110 (1980).

[31] B. Alles, M. D'Elia, and A. Di Giacomo, Phys. Lett. B **412**, 119 (1997).

[32] L. D. McLerran, E. Mottola, and M. E. Shaposhnikov, Phys. Rev. D **43**, 2027 (1991).

[33] Notice that in a quenched theory the electromagnetic Debye screening is less effective compared to a theory with virtual quarks because of the absence of the quark pair creation in the quenched case.

[34] P. W. Anderson, Phys. Rev. **109**, 1492 (1958).